

Edge Information Hub: Orchestrating Satellites, UAVs, MEC, Sensing and Communications for 6G Closed-Loop Controls

Chengleyang Lei, *Student Member, IEEE*, Wei Feng, *Senior Member, IEEE*, Peng Wei, *Member, IEEE*, Yunfei Chen, *Senior Member, IEEE*, Ning Ge, *Member, IEEE*, and Shiwen Mao, *Fellow, IEEE*

Abstract—An increasing number of field robots would be used for mission-critical tasks in remote or post-disaster areas. Due to usually-limited individual abilities, these robots require an edge information hub (EIH), which is capable of not only communications but also sensing and computing. Such EIH could be deployed on a flexibly-dispatched unmanned aerial vehicle (UAV). Different from traditional aerial base stations or mobile edge computing (MEC), the EIH would direct the operations of robots via sensing-communication-computing-control (SC^3) closed-loop orchestration. This paper aims to optimize the closed-loop control performance of multiple SC^3 loops, under the constraints of satellite-backhaul rate, computing capability, and on-board energy. Specifically, the linear quadratic regulator (LQR) control cost is used to measure the closed-loop utility, and a sum LQR cost minimization problem is formulated to jointly optimize the splitting of sensor data and allocation of communication and computing resources. We first derive the optimal splitting ratio of sensor data, and then recast the problem to a more tractable form. An iterative algorithm is finally proposed to provide a sub-optimal solution. Simulation results demonstrate the superiority of the proposed algorithm. We also uncover the influence of SC^3 parameters on closed-loop controls, highlighting more systematic understanding.

Index Terms—Closed-loop control, edge information hub (EIH), linear quadratic regulator (LQR), satellite, unmanned aerial vehicle (UAV).

I. INTRODUCTION

Robots and various unmanned machines have great potential to help humans carry out dangerous and strenuous tasks in post-disaster or remote areas [1], [2]. In general, the abilities of an individual robot are usually limited. For example, the sensors equipped on a robot could only detect its surrounding information. The onboard computers may malfunction due to the electronic components failure caused by the harsh conditions after disasters, including high temperatures and radiation [3]. In such cases, the robots have to rely on external helpers to assist them with mission-critical control tasks. Such

helper should be integrated with sensing functionality for global environmental detection [4], computing functionality for sensor-data analysis and decision-making [5], and communication functionality for delivering control commands [6].

As an integrated center of the control-oriented information, we refer to the above helper as edge information hub (EIH), which incorporates remote sensors, mobile edge computing (MEC) servers and communication modules. Note that, the terrestrial infrastructures may be unavailable during disasters. For more robust applications, the EIH can be deployed on a flexibly-dispatched unmanned aerial vehicle (UAV) in an on-demand manner. In addition, the payload of an EIH is limited in practice, resulting in sometimes-limited computing capability onboard. Accordingly, the satellite could be leveraged to offload some sensor data to the remote cloud. This leads to EIH-based satellite-UAV networks for control tasks.

The EIH assists the field robots to accomplish control tasks in a closed-loop manner. Specifically, the remote sensors collect information of the controlled objects, and then the computing modules (comprising the MEC server and the remote cloud via satellite) process the sensor data for decision making and generating control commands. Next, the communication modules transmit the commands to the corresponding robots. Finally, the robots follow the commands to perform the tasks. This entire process is referred to as the sensing-communication-computing-control (SC^3) loop [7]. Different parts of the SC^3 loop are coupled with each other. Therefore, different from the traditional system design focusing on communications only, it becomes more relevant to focus on the whole closed-loop performance and to design different parts of the SC^3 loop with a systematic mindset. In addition, constrained by the payload of UAVs, both communication and computing resources on the EIH are limited [8]–[10]. It is necessary to orchestrate the communication and computing resources to ensure that resource allocation aligns with control requirements. Motivated by these considerations, we investigate the joint communication and computing resource allocation problem of an EIH serving multiple robots for their control tasks, with the aim of optimizing the closed-loop control performance.

A. Related Works

Closed-loop control utilizes the output of a dynamic system as the input of the controller, which forms a closed loop [11]. It

Chengleyang Lei, Wei Feng, and Ning Ge, are with the Department of Electronic Engineering, Beijing National Research Center for Information Science and Technology, Tsinghua University, Beijing 100084, China (email: lcly21@mails.tsinghua.edu.cn, fengwei@tsinghua.edu.cn, gening@tsinghua.edu.cn).

Peng Wei is with the National Key Laboratory of Science and Technology on Communications, University of Electronic Science and Technology of China, Chengdu 611731, China (e-mail: wppisces@uestc.edu.cn).

Yunfei Chen is with the Department of Engineering, University of Durham, DH1 3LE Durham, U.K. (e-mail: yunfei.chen@durham.ac.uk).

Shiwen Mao is with the Department of Electrical and Computer Engineering, Auburn University, Auburn, AL 36849, USA (e-mail: smao@ieee.org).

is an important research field in the control theory, as it can stabilize an unstable system and reduce sensitivity to disturbance [12]. Classical control theory, rooted in frequency domain techniques based on transfer functions, has been extensively investigated [13], [14]. In the late 1950s, researchers began to develop the modern control theory, employing the state variable approach [15], [16]. An important area within modern control theory is optimal control, which aims at seeking a control strategy that optimizes an objective function [17], [18]. In optimal control, the linear quadratic regulator (LQR) control cost is commonly used to measure the system state deviation and control input energy [19]. The optimal control strategy to minimize the LQR cost has been proven to be a linear strategy [20]. Nevertheless, most works in the control field assume that the communication limitations in the loops have a negligible impact on control performance [21]. However, the communication resources on the EIH are usually limited by the UAV payload and flight time. In such cases, the impact of communication limitations in the SC^3 loops becomes non-negligible. Therefore, it is necessary to take the limitations of communication capability into consideration.

Networked control systems (NCSs), wherein the control systems are connected through a communication network, have been recently studied due to their flexibility and maintainability [22], [23]. Many works have been conducted to investigate the impact of communication limitations on the control system stability from various aspects, including data rate [21], delay [24], packet loss [25], [26], and so on. In [21], the authors demonstrated that the control system can be stabilized only if the communication data rate exceeds its intrinsic entropy rate. Ref. [24] investigated a NCS consisting of clock-driven sensors and event-driven controllers and actuators, and analyzed the stability region plot with respect to the sampling rate and network-induced delay. Authors in [25] considered the logarithmic quantization and packet loss and derived the stability condition. Ref. [26] further considered the packet loss and random delays in NCSs. A set of necessary and sufficient conditions for stabilizing the NCSs were proposed. On the other hand, some works designed control strategies contemplating communication limitations [27]–[31]. A control strategy aiming at achieving good performance over an unreliable communication network affected by packet loss and delays was described in [27], which uses the data packet frame to transmit control sequences. The authors in [28] proposed an event-triggered control strategy that guaranteed stability with an H_∞ norm bound, where the communication delay was considered. In [29], the control strategy and transmit power policies were designed to minimize the weighted sum of the control cost and power cost, where the packet loss was considered. Ref. [30] investigated the tradeoff between the data rate and the control performance. The transmission and control strategies were proposed to minimize the sum of the communication cost and control cost function. Authors in [31] considered the packet loss and optimized control parameters under the system instability probability constraint. In addition, some works investigated the influence of communication indicators on control performance [32]–[34]. In [32], a lower bound of the minimum average data

rate to achieve a certain LQR cost was presented. Authors in [33] investigated connected and automated vehicles, where the impact of communication erasure channels on vehicle platoon formation and robustness was analyzed. Ref. [34] further investigated the tradeoff between the average data rate and control performance of NCSs, considering the transmission delay. All of these works are valuable for analyzing the SC^3 loops. However, most of these works only investigated one control loop from the perspectives of performance analysis or control strategy design, instead of resource allocation among multiple SC^3 loops.

Recently, some works have been conducted on the communication resource allocation among SC^3 loops considering the control performance [7], [35], [36]. The authors in [35] studied the resource allocation problem in wireless control systems, where the bandwidth and transmit power were jointly optimized to maximize the spectral efficiency, under the control convergence rate constraint. Ref. [36] designed a frequency allocation policy to keep the overall control system stable. In our previous work [7], we formulated an LQR cost minimization problem that optimized the transmit power allocation. However, these works did not utilize MEC or consider the computing resource allocation to reduce latency.

On the other hand, the UAV-aided MEC has been widely investigated as a potential technology to extend the coverage of computation service [37]–[40]. The authors in [37] considered a UAV-aided MEC system, where the user data can be processed locally or offloaded to the MEC. The sum of delays was minimized by jointly optimizing the UAV trajectory, the ratio of offloading tasks, and the user scheduling variables. The author in [38] further proposed a multi-agent reinforcement learning based method to solve the resource allocation problem in an MEC- and UAV-assisted vehicular network. Ref. [39] considered the information security in the UAV-assisted MEC system, where the secure computation efficiency was maximized by optimizing the offloading decision and resource allocation based on deep reinforcement learning. The authors in [40] investigated a vehicular edge computing system, where a UAV was utilized to assist task offloading. A UAV-assisted vehicular task offloading problem was proposed to minimize vehicular task delay. Most existing works on the UAV-aided MEC focus on communication performance, such as latency or energy efficiency. However, in SC^3 loops, our concern is the overall closed-loop control performance, rather than the separate communication or computing performances. Therefore, the closed-loop performance is of more interest to the system design.

B. Main Contributions

Motivated by the above observations, in this paper, we investigate an EIH-empowered SC^3 system where an EIH assists multiple robots for their control tasks. The UAV-mounted EIH integrates the sensing, computing, and communication capabilities to assist the robots, and utilizes satellite to backhaul data. We jointly optimize the communication and computing resources, as well as the splitting vector of sensor data, to minimize the sum LQR cost of multiple loops. The

optimization problem is a non-convex problem. We recast it to a more tractable form and propose an iterative algorithm to solve it. The main contributions are summarized as follows.

- We consider a UAV-mounted EIH, which is integrated with a remote sensor, an MEC server, and a communication module to assist multiple robots with their control tasks. The sensor data can be processed locally on EIH, offloaded to the cloud after pre-processing, or offloaded to the cloud without pre-processing. In order to explore the potential of closed-loop orchestration, we jointly optimize the splitting of sensor data and allocation of communication and computing resources. Specifically, we utilize the LQR cost to evaluate the overall control performance, and incorporate the minimum information entropy constraint to achieve a certain LQR cost.
- We formulate a sum LQR cost minimization problem, which jointly optimizes the splitting vector of sensor data, the computing capability of MEC, the satellite-backhaul rate, and the transmit power from EIH to robots. The problem is non-convex. We derive the optimal splitting vector of sensor data, and accordingly recast the original problem to a more tractable form. Finally, we propose an iterative algorithm to solve the recast problem based on the successive convex approximation (SCA) method.
- We provide simulation results to show the superiority of the proposed closed-loop-oriented method over the traditional communication-oriented method. Additionally, we show how the sensing noise variance and the computing capability influence the LQR cost through simulation.

C. Organization and Notation

The rest of the paper is organized as follows. Section II introduces the system model, and formulates the optimization problem. In Section III, we recast the original problem to a more tractable form and propose an iterative algorithm to solve it. Simulation results are provided in Section IV with further discussions. Finally, Section V concludes this paper.

Throughout this paper, lower case and upper case boldface symbols denote vectors and matrices, respectively. \mathbb{R}^n represents the collection of all the n -dimensional real-number vectors, and $\mathbb{R}^{m \times n}$ represents the collection of all the $m \times n$ real-number matrices. \mathbb{E} is the expectation operator. $\text{tr}\{\cdot\}$ and $\det\{\cdot\}$ denote the trace operator and the determinant operator, respectively.

II. SYSTEM MODEL AND PROBLEM FORMULATION

As shown in Fig. 1, we consider an EIH-empowered SC^3 system, where K field robots are assisted by the EIH to perform mission-critical tasks. The UAV-mounted EIH incorporates a remote sensing module, an MEC server, and a communication module to synergistically integrate sensing, computing, and communication functions. Due to the limited computing capability on the EIH, part of the sensor data will be offloaded to the cloud center through the satellite.

The EIH directs the field robots by forming SC^3 closed loops. In each loop, the remote sensor captures the states of the controlled object. The sensor data is then processed on the

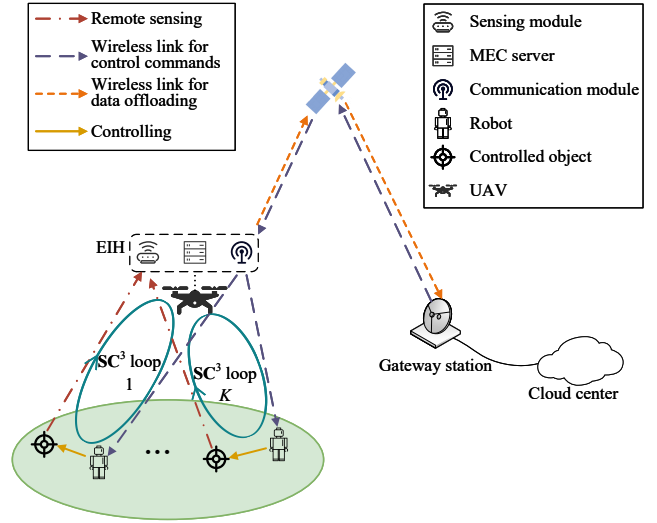


Fig. 1. Illustration of an EIH-empowered SC^3 system, where the EIH is mounted on a UAV, and utilizes satellites to backhaul data.

MEC server or on the cloud to judge the situation and make corresponding control commands. Next, the communication module sends these commands to the field robots. The field robots follow the received commands to handle its object. The whole process is performed periodically. In the following, we will detail the models of different parts of the SC^3 loop.

A. Computation Model

In each cycle, the sensor data are analyzed to compute the optimal control commands. Due to the limited computing capability of the MEC server in the EIH, some of the sensor data will be offloaded to the cloud through satellite. As shown in Fig. 2, we assume the sensor data can be arbitrarily split into three parts:

- Part 1: processed on the MEC server completely.
- Part 2: pre-processed in the MEC server and then transmitted to the cloud for further processing.
- Part 3: processed in the cloud completely.

The data sizes of the three parts of the sensor data in loop k are denoted as $D_{k,1}$, $D_{k,2}$ and $D_{k,3}$ in bits. We have

$$D_{k,1} + D_{k,2} + D_{k,3} = D_k, \quad (1)$$

where D_k denotes the total size of the sensor data of SC^3 loop k in each cycle.

The three parts of sensor data are processed in parallel as data streams. The overall computation time depends on the maximum processing time of the three parts.

For the first part of sensor data, the computation time can be formulated as

$$T_{k,1}^{\text{comp}} = \frac{\alpha D_{k,1}}{f_{k,1}}, \quad (2)$$

where α denotes the number of CPU cycles for processing the sensor data per bit, and $f_{k,1}$ is the computing capability (i.e., CPU frequency) allocated to part 1 in loop k by the MEC.

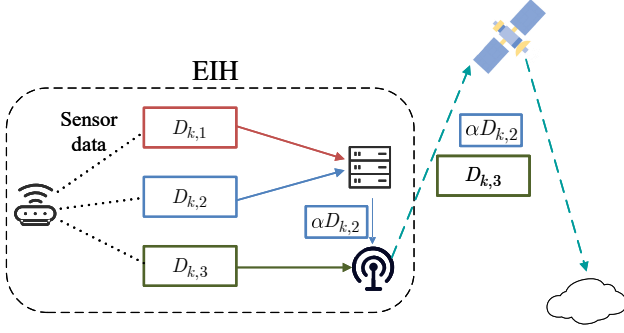


Fig. 2. Illustration of three flows of the remote sensor data.

For the second part of sensor data, the data are first pre-processed on the MEC server, where the processing time can be calculated as

$$T_{k,2}^{\text{proc}} = \frac{\beta D_{k,2}}{f_{k,2}}, \quad (3)$$

where β denotes the number of CPU cycles for pre-processing sensor data per bit, and $f_{k,2}$ is the computing capability allocated to Part 2 in loop k by the MEC server.

We assume the data compression ratio of pre-processing is ρ , i.e., data of $\rho D_{k,2}$ bits will be transmitted to the satellite for further processing after pre-processing. The transmission latency from the UAV to satellite can be calculated as

$$T_{k,2}^{\text{trans}} = \frac{\rho D_{k,2}}{R_{k,2}}, \quad (4)$$

where $R_{k,2}$ is the transmission data rate from UAV to satellite allocated to Part 2 in loop k .

The downlink transmission data rate from the satellite to the cloud is usually much bigger than the uplink data rate. Therefore, the downlink transmission latency is negligible compared with $T_{k,2}^{\text{trans}}$. In addition, we assume that the cloud has enough computing capability, so that the computation time on satellite is negligible. The transmission latency of the output data is also assumed to be ignorable as the output data is much smaller than the input data size. Based on the above analysis, the overall time for processing the second part of sensor data can be calculated as

$$T_{k,2}^{\text{comp}} = \begin{cases} 0, & \text{if } D_{k,2} = 0 \\ \max \{T_{k,2}^{\text{proc}}, T_{k,2}^{\text{trans}}\} + 4\tau, & \text{if } D_{k,2} > 0 \end{cases} \quad (5)$$

where τ is the propagation latency between the ground and the satellite. The pre-processing and the transmission process are performed in parallel. Therefore, the overall latency will be determined by the maximum of the two processes. It should be noted that we have considered the special case of $D_{k,2} = 0$, i.e., we do not split any data to Part 2. In such case, the latency for data of Part 2 is zero.

For the data in Part 3, similarly, the total time can be

calculated as

$$T_{k,3}^{\text{comp}} = \begin{cases} 0, & \text{if } D_{k,3} = 0 \\ \frac{D_{k,3}}{R_{k,3}} + 4\tau, & \text{if } D_{k,3} > 0, \end{cases} \quad (6)$$

where $R_{k,3}$ is the satellite-backhaul rate allocated to the data of part 3 in loop k .

In conclusion, the overall time duration of the computing phase can be formulated as

$$T_k^{\text{comp}} = \max \{T_{k,1}^{\text{comp}}, T_{k,2}^{\text{comp}}, T_{k,3}^{\text{comp}}\}. \quad (7)$$

Considering the limited computation and communication resources, we have the following constraints

$$\sum_{k=1}^K (f_{k,1} + f_{k,2}) \leq F_{\max}, \quad (8)$$

$$\sum_{k=1}^K (R_{k,2} + R_{k,3}) \leq R_{\max}^{\text{U2S}}, \quad (9)$$

where F_{\max} denotes the computing capability of the MEC server, and R_{\max}^{U2S} denotes the maximum satellite-backhaul rate.

B. Communication Model

After processing the sensor data, the control commands will be transmitted to the field robots. The EIH transmits the control commands to K robots simultaneously through orthogonal channels. Denoting the transmit power allocated to loop k as p_k , we have

$$\sum_{k=1}^K p_k \leq P_{\max}, \quad (10)$$

where P_{\max} represents the transmit power constraint.

The EIH communications with satellites and field robots in different frequency bands, so we assume that there is no communication interference among different communication links. The wireless channels between the EIH and robots are assumed to be dominated by line-of-sight (LoS) links [41]. Therefore, the channel gain from the EIH to robot k follows the free space path loss model as $g_k = \frac{\gamma_0}{d_k^2}$, where d_k denotes the distance from the UAV to robot k and γ_0 is the reference channel gain at the distance of one meter. The transmit data rate from EIH to robot k can be calculated as

$$R_k^{\text{U2G}}(p_k) = \log_2 \left(1 + \frac{g_k p_k}{\sigma^2} \right), \quad (11)$$

where σ^2 denotes the channel noise power.

The computing phase and communication phase of each loop share the time resource, which can be denoted as

$$T_k^{\text{comp}} + T_k^{\text{commu}} \leq T_k, \quad (12)$$

where T_k^{commu} denotes the transmission time of the control commands, and T_k is the time resource reserved for the computing and communication phase, which is assumed to be fixed in each cycle.

C. Control Model

After receiving the control commands from the EIH, the robots follow the commands to handle the objects. For simplicity, we model each robot and its object as a linear control system¹, and formulate the discrete-time system equation of the k -th control system in cycle t as [32]

$$\mathbf{x}_{k,t+1} = \mathbf{A}_k \mathbf{x}_{k,t} + \mathbf{B}_k \mathbf{u}_{k,t} + \mathbf{v}_{k,t}, \quad (13)$$

where t denotes the cycle index, $\mathbf{x}_{k,t} \in \mathbb{R}^{n_k}$ denotes the system state, such as the temperature or radiation intensity, $\mathbf{u}_{k,t} \in \mathbb{R}^{m_k}$ denotes the control input, n_k and m_k denote the dimensions of the system state and control input, respectively, $\mathbf{v}_{k,t} \in \mathbb{R}^{n_k}$ denotes Gaussian system noise with mean zero and covariance Σ_k^v , and \mathbf{A}_k and \mathbf{B}_k are fixed $n_k \times n_k$ and $n_k \times m_k$ matrices denoting the state matrix and input matrix.

We also consider a linear sensing model, where the observation equation can be written as

$$\mathbf{y}_{k,t} = \mathbf{C}_k \mathbf{x}_{k,t} + \mathbf{w}_{k,t}, \quad (14)$$

where $\mathbf{y}_{k,t} \in \mathbb{R}^{q_k}$ is the sensing output, $\mathbf{C}_k \in \mathbb{R}^{q_k \times n_k}$ is the observation matrix, q_k denotes the dimension of the sensing output, and $\mathbf{w}_{k,t} \in \mathbb{R}^{q_k}$ is the Gaussian sensing noise with mean zero and covariance Σ_k^w .

In this paper, we evaluate the control performance with the infinite-horizon LQR cost [32], which is formulated as

$$l_k \triangleq \lim_{N \rightarrow \infty} \mathbb{E} \left[\sum_{t=1}^N (\mathbf{x}_{k,t}^T \mathbf{Q}_k \mathbf{x}_{k,t} + \mathbf{u}_{k,t}^T \mathbf{R}_k \mathbf{u}_{k,t}) \right], \quad (15)$$

where \mathbf{Q}_k and \mathbf{R}_k are semi-positive definite weight matrices. The term $\mathbf{x}_{k,t}^T \mathbf{Q}_k \mathbf{x}_{k,t}$ denotes the deviation of the system from zero state, and the term $\mathbf{u}_{k,t}^T \mathbf{R}_k \mathbf{u}_{k,t}$ denotes the control energy consumption. The weight matrices \mathbf{Q}_k and \mathbf{R}_k balance the state and the energy, which can be set according to the practical requirements.

As in (15), the LQR cost is determined by the system state $\mathbf{x}_{k,t}$ and the control input $\mathbf{u}_{k,t}$, which is mainly influenced by the control strategy that computes the control input based on the sensing output. We will not try to optimize the control strategy, which is beyond the scope of this work. Instead, we will focus on the impact of the communication ability on the LQR cost, and accordingly carry out computing and communication resource allocation.

We use the information entropy transmitted from the EIH to the robots per cycle to evaluate the communication capability. According to [32, Theorem 5], in order to achieve a certain LQR cost l_k , the information entropy transmitted through channel k in one cycle must satisfy the following constraint

$$BT_k^{\text{commu}} R_k^{\text{U2G}}(p_k) \geq \bar{e}_k(l_k), \quad (16)$$

where the left side of (16) denotes the maximum information entropy transmitted per cycle, and

$$\bar{e}_k(l_k) \triangleq h_k + \frac{n_k}{2} \log_2 \left(1 + \frac{n_k |\det \mathbf{N}_k \mathbf{M}_k|^{\frac{1}{n_k}}}{l_k - l_{\min,k}} \right) \quad (17)$$

¹Although some control systems may be quite complicated, they can still be analyzed as a linear system through local linearization [42].

denotes the minimum entropy to achieve LQR cost l_k , $h_k \triangleq \log_2 |\det \mathbf{A}_k|$ is the intrinsic entropy rate of object k . It should be noted that h_k evaluates the stability of object k . An object with a larger intrinsic entropy rate is more difficult to stabilize [21]. The term $l_{\min,k} = \text{tr}(\Sigma_k^v \mathbf{S}_k) + \text{tr}(\Sigma_k \mathbf{A}_k^T \mathbf{M}_k \mathbf{A}_k)$ denotes the lower bound of the LQR cost, where \mathbf{N}_k , \mathbf{M}_k and \mathbf{S}_k are the solutions to the matrix equations shown in [32], which are related to the control parameters, i.e., \mathbf{A}_k , \mathbf{B}_k , \mathbf{R}_k , \mathbf{Q}_k , Σ_k^v , and Σ_k^w .

D. Problem Formulation

In this work, we aim to minimize the sum LQR cost of the \mathbf{SC}^3 loops by jointly optimizing the transmit power allocation $\mathbf{p} = \{p_k\}$, the computing capability allocation $\mathbf{f} = \{f_{k,i}\}$, the satellite transmission rate allocation $\mathbf{R} = \{R_{k,j}\}$, and the data split vector $\mathbf{D} = \{D_{k,r}\}$ (where $i \in \{1, 2\}$, $j \in \{2, 3\}$ and $r \in \{1, 2, 3\}$), while keeping the information entropy constraint satisfied. The optimization problem is formulated as

$$\min_{\mathbf{p}, \mathbf{f}, \mathbf{R}, \mathbf{D}} \sum_{k=1}^K l_k \quad (18a)$$

$$\text{s.t.} \quad \sum_{k=1}^K p_k \leq P_{\max}, \quad (18b)$$

$$D_{k,1} + D_{k,2} + D_{k,3} = D_k, \quad k = 1, 2, \dots, K, \quad (18c)$$

$$\sum_{k=1}^K (f_{k,1} + f_{k,2}) \leq F_{\max}, \quad (18d)$$

$$\sum_{k=1}^K (R_{k,2} + R_{k,3}) \leq R_{\max}^{\text{U2S}}, \quad (18e)$$

$$T_k^{\text{comp}} + T_k^{\text{commu}} \leq T_k, \quad k = 1, 2, \dots, K, \quad (18f)$$

$$BT_k^{\text{commu}} R_k^{\text{U2G}}(p_k) \geq \bar{e}_k(l_k), \quad (18g)$$

where $\mathbf{l} = [l_1, l_2, \dots, l_K]$. The problem in (18) is non-convex due to the non-convex and non-continuous expression of T_k^{comp} as in (7). Therefore, it is difficult to solve (18) directly. Next, we will recast this problem to an equivalent and more tractable form by decoupling the optimization of data splitting vector \mathbf{D} .

III. PROBLEM TRANSFORMATION AND ITERATIVE SOLUTION

In this section, we will derive the optimal data splitting vector, given the computing capability and uplink transmission rate, so that we can decouple the optimization of \mathbf{D} , and find a way to recast the original problem more tractable. Then, based on the simplified optimization problem, we propose an iterative algorithm to obtain a sub-optimal solution.

A. Problem Transformation

It can be seen from (18) that the LQR cost l_k is influenced by the other variables only through the information entropy constraint (18g). As $\bar{e}_k(l_k)$ is decreasing with l_k , we can prove that l_k is increasing with the computation time T_k^{comp} .

Therefore, minimizing the LQR cost l_k in \mathbf{SC}^3 loop k is equivalent to minimizing the computation time T_k^{comp} . In addition, it is observed that the data splitting parameters in different \mathbf{SC}^3 loops are decoupled with each other. Therefore, if the computing and communication resources allocated to \mathbf{SC}^3 loop k is given, the optimal data splitting vector in that loop can be calculated by minimizing the computation time. Based on the above analysis, we can transform the optimization problem (18) to

$$\min_{\mathbf{p}, \mathbf{f}', \mathbf{R}', \mathbf{l}} \sum_{k=1}^K l_k \quad (19a)$$

$$\text{s.t.} \quad \sum_{k=1}^K p_k \leq P_{\max}, \quad (19b)$$

$$\sum_{k=1}^K f_k \leq F_{\max}, \quad (19c)$$

$$\sum_{k=1}^K R_k \leq R_{\max}^{\text{U2S}}, \quad (19d)$$

$$T_k^{\text{comp},*}(f_k, R_k) + T_k^{\text{commu}} \leq T_k, \quad k = 1, 2, \dots, K, \quad (19e)$$

$$BT_k^{\text{commu}} R_k^{\text{U2G}}(p_k) \geq \bar{e}_k(l_k), \quad (19f)$$

where $f_k = f_{k,1} + f_{k,2}$ denotes the overall computing capability allocated to \mathbf{SC}^3 loop k , $\mathbf{R}' = \{R_k\}$ denotes the satellite transmission rate allocated to \mathbf{SC}^3 loop k , and $\mathbf{f}' = \{f_k\}$ and $\mathbf{R}' = \{R_k\}$. The function $T_k^{\text{comp},*}(f_k, R_k)$ denotes the minimal computation time of loop k when f_k and R_k are given. $T_k^{\text{comp},*}(f_k, R_k)$ can be calculated as the optimal objective function value of the following optimization problem

$$\min_{\mathbf{D}_k, \mathbf{f}_k, \mathbf{R}_k} \max \{T_{k,1}^{\text{comp}}, T_{k,2}^{\text{comp}}, T_{k,3}^{\text{comp}}\}. \quad (20a)$$

$$\text{s.t.} \quad D_{k,1} + D_{k,2} + D_{k,3} = D_k, \quad (20b)$$

$$f_{k,1} + f_{k,2} \leq f_k, \quad (20c)$$

$$R_{k,2} + R_{k,3} \leq R_k \quad (20d)$$

where $\mathbf{D}_k = \{D_{k,1}, D_{k,2}, D_{k,3}\}$, $\mathbf{f}_k = \{f_{k,1}, f_{k,2}\}$ and $\mathbf{R}_k = \{R_{k,2}, R_{k,3}\}$ denote the split schemes in \mathbf{SC}^3 loop k . The equivalence of (18) and (19) can be obtained from the monotonicity of (18g). The optimization problem (20) is non-convex due to the non-convex and non-continuous objective function. Next, we will solve the problem (20) and give a closed-form expression of $T_k^{\text{comp},*}(f_k, R_k)$.

B. Optimal Solution to Problem (20)

The problem in (20) is not convex and therefore difficult to solve directly. In order to solve (20), we have the following lemma.

Lemma 1: If $f_k < \frac{\alpha D_k}{4\tau}$, then the equations

$$T_{k,1}^{\text{comp}} = T_{k,2}^{\text{comp}} = T_{k,3}^{\text{comp}}, \quad (21)$$

$$T_{k,2}^{\text{proc}} = T_{k,2}^{\text{trans}} \quad (22)$$

must hold in order to minimize the computation time in \mathbf{SC}^3 loop k .

Proof: From (2), (5) and (6), we can see that the computation time of each part of sensor data is strictly increasing with the respective data size, i.e., $D_{k,1}$, $D_{k,2}$ and $D_{k,3}$. Therefore, if (21) does not hold and $T_{k,i}$ ($i \in \{1, 2, 3\}$) is larger than the other two terms, then we have $T_k^{\text{comp}} = T_{k,i}^{\text{comp}}$. We can reduce the corresponding data size $D_{k,i}$ and increase the data size of the other two parts, until (21) holds. Following the above procedure, we decrease $T_{k,i}^{\text{comp}}$ and increase the computation time of the other two parts, and thereby decreasing the overall computation time T_k^{comp} . Therefore, the equation (21) must hold to minimize the overall computation time if $f_k < \frac{\alpha D_k}{4\tau}$ (the condition $f_k < \frac{\alpha D_k}{4\tau}$ guarantees that $T_k^{\text{comp},*} > 4\tau$ and increasing the data size of Part 2 or Part 3 at the jumping point, i.e., the zero pint, will not increase the overall computation time).

Next, we prove that (22) should hold to minimize T_k^{comp} . If $T_{k,2}^{\text{comp}} > T_{k,2}^{\text{trans}}$, which indicates that the communication resource for the second part of sensor data in loop k is redundant, we can decrease $R_{k,2}$ and increase $R_{k,3}$ until (22) holds. The above procedure will decrease $T_{k,3}^{\text{comp}}$ while maintaining $T_{k,2}^{\text{comp}}$ unchanged, resulting in a non-increasing overall computation time T_k^{comp} . On the other hand, if $T_{k,2}^{\text{comp}} < T_{k,2}^{\text{trans}}$, we can decrease $f_{k,2}$ and increase $f_{k,1}$ in a similar way to ensure that T_k^{comp} is non-increasing. \square

Based on **Lemma 1**, we have the following proposition in the next page.

Proposition 1: The optimal value of the objective function of (20) is given by the piece-wise function shown in (23) on the next page.

Proof: See Appendix A. \square

Remark 1: In most cases, all the computing and communication resources allocated to \mathbf{SC}^3 loop k will be utilized, and $T_k^{\text{comp},*}$ is strictly decreasing with respect to f_k and R_k . The exception is when $f_k \geq \frac{\alpha D_k}{4\tau}$, which indicates that the MEC computing capability is enough and the computation time on the MEC server is less than the satellite propagation delay. In such case, all the sensor data will be processed on the EIH, and the satellite communication resource will not be utilized even if R_k is large.

Remark 2: In the case when $\alpha - \alpha\rho - \beta < 0$, we have $\mathcal{S}_1 = \mathcal{S}_2 = \emptyset$. In such case, we have $D_{k,2} = 0$, i.e., none of the sensor data will be pre-processed on the MEC server. In fact, the condition $m - m\rho - n < 0$ holds if n is close to m or ρ is close to 1, which implies that pre-processing the sensing is not so useful.

C. Joint Communication and Computing Resource Optimization

Based on **Proposition 1**, we can remove the optimization variables \mathbf{D} and recast (18) to an equivalent form as (19). However, (19) is still a non-convex optimization problem due to the non-convexity of $T_k^{\text{comp},*}(f_k, R_k)$. Next, we propose an iterative algorithm to solve the joint communication and computing resource optimization problem

$$T_k^{\text{comp},*}(f_k, R_k) = \begin{cases} T_k^1(f_k, R_k) \triangleq \frac{\beta D_k}{\beta R_k + (1-\rho)f_k} + 4\tau, & (f_k, R_k) \in \mathcal{S}_1 \triangleq \left\{ (f, R) \mid 0 \leq f \leq \min \left\{ \frac{(\alpha - \alpha\rho - \beta)D_k - 4\beta\tau R}{4(1-\rho)\tau}, \frac{\beta R}{\rho} \right\} \right\} \\ T_k^2(f_k, R_k) \triangleq \frac{\rho\alpha D_k - 4\rho\tau f_k + 4\beta R_k\tau}{\rho f_k + (\alpha - \beta)R_k} + 4\tau, & (f_k, R_k) \in \mathcal{S}_2 \triangleq \left\{ (f, R) \mid \frac{\beta R}{\rho} \leq f \leq \frac{(\alpha - \alpha\rho - \beta)D_k - 4\beta\tau R}{2(1-\rho)\tau}, R \geq 0 \right\} \\ T_k^3(f_k, R_k) \triangleq \frac{\alpha D_k - 4\tau f_k}{f_k + \alpha R_k} + 4\tau, & (f_k, R_k) \in \mathcal{S}_3 \triangleq \left\{ (f, R) \mid \frac{(\alpha - \alpha\rho - \beta)D_k - 4\beta\tau R}{4(1-\rho)\tau} \leq f \leq \frac{\alpha D_k}{4\tau}, f \geq 0, R \geq 0 \right\} \\ T_k^4(f_k, R_k) \triangleq \frac{\alpha D_k}{f_k}, & (f_k, R_k) \in \mathcal{S}_4 \triangleq \left\{ (f, R) \mid f \geq \frac{\alpha D_k}{4\tau}, R \geq 0 \right\} \end{cases} \quad (23)$$

First, we regard the communication time $\{T_k^{\text{commu}}\}$ as optimization variables, and rewrite (19) as

$$\min_{\mathbf{p}, \mathbf{f}', \mathbf{R}', \mathbf{l}, \mathbf{T}^{\text{commu}}} \sum_{k=1}^K l_k \quad (24a)$$

$$\text{s.t.} \quad \sum_{k=1}^K p_k \leq P_{\max}, \quad (24b)$$

$$\sum_{k=1}^K f_k \leq F_{\max}, \quad (24c)$$

$$\sum_{k=1}^K R_k \leq R_{\max}^{\text{U2S}} \quad (24d)$$

$$T_k^{\text{comp},*}(f_k, R_k) + T_k^{\text{commu}} \leq T_k, \quad k = 1, 2, \dots, K, \quad (24e)$$

$$BR_k^{\text{U2G}}(p_k) \geq \frac{\bar{e}_k(l_k)}{T_k^{\text{commu}}}, \quad k = 1, 2, \dots, K, \quad (24f)$$

where $\mathbf{T}^{\text{commu}} = \{T_k^{\text{commu}}\}$. By regarding T_k^{commu} as a variable and moving it to the left of (24f), we can clarify the convexity of (24), based on the following lemma.

Lemma 2: The function $f(x, y) = \frac{1}{y} \log \left(1 + \frac{1}{x-a} \right)$ with $a \in \mathbb{R}^+$ is convex in the domain $\text{dom} f = \{(x, y) \mid x > a, y > 0\}$.

Proof: See Appendix B. \square

Based on **Lemma 2**, it can be shown that the right side of (24e), i.e., $\bar{e}_k(l_k)/T_k^{\text{commu}}$, is convex with respect to l_k and T_k^{commu} . In addition, we have $R_k^{\text{U2G}}(p_k)$ is concave with respect to p_k . Therefore, constraint (24e) describes a convex set. However, the function $T_k^{\text{comp},*}(f_k, R_k)$ in (24e) is piece-wise and non-convex, which makes this problem still difficult to solve. Next, we propose an iterative algorithm to solve (24) based on the SCA method [44]. Before proceeding further, we introduce the following lemma in order to approximate the non-convex function $T_k^{\text{comp},*}(f_k, R_k)$.

Lemma 3: For the convex function $1/xy$ with $x > 0$ and $y > 0$, we have the following inequality for any $x_0 > 0$ and $y_0 > 0$

$$\frac{1}{xy} \geq \frac{1}{x_0 y_0} \left(3 - \frac{x}{x_0} - \frac{y}{y_0} \right). \quad (25)$$

Proof: The convexity can be checked of $1/xy$ by checking the Hessian matrix. With the convexity of $1/xy$, we can obtain the inequality in (25) immediately through the first-order condition of convex functions [43, Section 3.1.3]. \square

Based on **Lemma 3**, we have the following inequality by substituting $x = 1/u, y = au + bv, x_0 = 1/u_0, y_0 = au_0 + bv_0$ into (25)

$$\frac{u}{au + bv} \geq \frac{u_0}{au_0 + bv_0} \left(3 - \frac{u_0}{u} - \frac{au + bv}{au_0 + bv_0} \right), \quad (26)$$

where $a > 0, b > 0, u > 0$ and $v > 0$.

With (26), we are ready to approximate $T_k^{\text{comp},*}(f_k, R_k)$ with a convex function. The approximate function $\bar{T}_k^{\text{comp},*}(f_k, R_k | f_{k0}, R_{k0})$ is formulated as (29) on the next page, where $f_{k0} > 0$ and $R_{k0} > 0$ are fixed values, and $\bar{T}_k^2(f_k, R_k | f_{k0}, R_{k0})$ and $\bar{T}_k^3(f_k, R_k | f_{k0}, R_{k0})$ are two convex functions that approximate $T_k^2(f_k, R_k)$ and $T_k^3(f_k, R_k)$, respectively, formulated as (30) and (32) on the next page. The inequalities in (31) and (33) follow from (26), indicating that

$$\bar{T}_k^2(f_k, R_k | f_{k0}, R_{k0}) \geq T_k^2(f_k, R_k), \quad (27)$$

$$\bar{T}_k^3(f_k, R_k | f_{k0}, R_{k0}) \geq T_k^3(f_k, R_k). \quad (28)$$

It should be noted that the approximate function $\bar{T}_k^{\text{comp},*}(f_k, R_k | f_{k0}, R_{k0})$ is not a piece-wise function. Instead, the specific expression of $\bar{T}_k^{\text{comp},*}(f_k, R_k | f_{k0}, R_{k0})$ depends on the values of f_{k0} and R_{k0} . We have the following lemma which illustrates the fundamental properties of $\bar{T}_k^{\text{comp},*}$.

Lemma 4: The function $\bar{T}_k^{\text{comp},*}(f_k, R_k | f_{k0}, R_{k0})$ shown in (29) is a convex function, and satisfies the following inequality

$$\bar{T}_k^{\text{comp},*}(f_k, R_k | f_{k0}, R_{k0}) \geq T_k^{\text{comp},*}(f_k, R_k), \quad (34)$$

where f_{k0} and R_{k0} are non-negative constants, and the equality holds if $f_k = f_{k0}$, and $R_k = R_{k0}$.

Proof: See Appendix C. \square

By approximating $T_k^{\text{comp},*}(f_k, R_k)$ with $\bar{T}_k^{\text{comp},*}(f_k, R_k | f_{k0}, R_{k0})$, we propose an iterative algorithm to obtain a sub-optimal solution to problem (24). During each iteration, we solve an approximate optimization problem of (24), formulated as

$$\min_{\mathbf{p}, \mathbf{f}', \mathbf{R}', \mathbf{l}, \mathbf{T}^{\text{commu}}} \sum_{k=1}^K l_k \quad (35a)$$

$$\bar{T}_k^{\text{comp},*}(f_k, R_k|f_{k0}, R_{k0}) = \begin{cases} \max \left\{ T_k^1(f_k, R_k), \bar{T}_k^2(f_k, R_k|f_{k0}, R_{k0}) \right\}, & (f_{k0}, R_{k0}) \in \mathcal{S}_1 \cup \mathcal{S}_2 \\ \bar{T}_k^3(f_k, R_k|f_{k0}, R_{k0}), & (f_{k0}, R_{k0}) \in \mathcal{S}_3 \\ T_k^4(f_k, R_k), & (f_{k0}, R_{k0}) \in \mathcal{S}_4 \end{cases} \quad (29)$$

$$\bar{T}_k^2(f_k, R_k|f_{k0}, R_{k0}) \triangleq \frac{\rho \alpha D_k}{\rho f_k + (\alpha - \beta) R_k} + 4 \frac{\alpha \tau}{\alpha - \beta} - \frac{\frac{4\rho\alpha\tau}{\alpha-\beta} f_{k0}}{\rho f_{k0} + (\alpha - \beta) R_{k0}} \left[3 - \frac{f_{k0}}{f_k} - \frac{\rho f_k + (\alpha - \beta) R_k}{\rho f_{k0} + (\alpha - \beta) R_{k0}} \right] \quad (30)$$

$$\geq \frac{\rho \alpha D_k}{\rho f_k + (\alpha - \beta) R_k} + 4 \frac{\alpha \tau}{\alpha - \beta} - \frac{\frac{4\rho\alpha\tau}{\alpha-\beta} f_k}{\rho f_k + (\alpha - \beta) R_k} \quad (31)$$

$$\bar{T}_k^3(f_k, R_k|f_{k0}, R_{k0}) \triangleq \frac{\alpha D_k}{f_k + \alpha R_k} + 4\tau - \frac{4\tau f_{k0}}{f_{k0} + \alpha R_{k0}} \left[3 - \frac{f_{k0}}{f_k} - \frac{f_k + \alpha R_k}{f_{k0} + \alpha R_{k0}} \right] \quad (32)$$

$$\geq \frac{\alpha D_k}{f_k + \alpha R_k} + 4\tau - \frac{4\tau f_k}{f_k + \alpha R_k} \quad (33)$$

Algorithm 1: The proposed iterative algorithm for solving problem (24)

Input : System parameter $P_{\max}, F_{\max}, R_{\max}$, etc; the convergence tolerance ϵ .

Initialization: Calculate a feasible \mathbf{f}^0 and \mathbf{R}^0 based on (35c) and (35d), and set $i = 0$

1 **repeat**

2 Set $i = i + 1$;

3 Update $\mathbf{p}^i, \mathbf{f}^i$ and \mathbf{R}^i by solving (35), denote the value of the objective function as L^i ;

4 **until** $\frac{L^{i-1} - L^i}{L^{i-1}} < \epsilon$;

Output : the optimal resource allocation $\mathbf{p}^i, \mathbf{f}^i, \mathbf{R}^i$, and the sum LQR cost L^i .

algorithm can be demonstrated with the following proposition.

Proposition 2: The output solution of **Algorithm 1** is a feasible solution to the optimization problem in (24). In addition, L^i in **Algorithm 1** is non-increasing along with the iterations, i.e., $L^{i-1} \geq L^i$ holds for any $i \geq 1$. Therefore, **Algorithm 1** is assured to converge.

Proof: See Appendix D. \square

The computational complexity of the proposed **Algorithm 1** to solve (24) is dominated by the process of solving (35) during the iterations. As (35) is a convex optimization problem, it can be solved with interior point method [43]. The complexity of the interior point method is $\mathcal{O}(K^{3.5} \log(1/\epsilon_0))$, where ϵ_0 is the solution accuracy of the interior point method [45]. Denoting the iteration number of **Algorithm 1** as I_1 , the overall computational complexity of the proposed algorithm is $\mathcal{O}(I_1 K^{3.5} \log(1/\epsilon_0))$. In the next section, we will evaluate the iteration numbers via simulations.

IV. SIMULATION RESULTS AND DISCUSSION

In this section, we provide simulation results to evaluate our proposed algorithm. We consider an EIH-empowered SC^3 system where the EIH assists $K = 5$ robots for their control tasks. The locations of the robots are assumed to be randomly distributed in a circular area with a radius of 5000 m. The UAV is located in the center of the circle, with the height of 100 m. The bandwidth of each channel is set as $B = 5\text{kHz}$, and other parameters are set as $\beta_0 = -60\text{ dB}$ and $\sigma^2 = -110\text{ dBm}$ [46]. We assume a Low Earth Orbit (LEO) satellite, with the height of 1500 km, and hence $\tau = 5\text{ ms}$. The power constraint and the satellite-backhaul rate constraint are set as $P_{\max} = 10\text{ dBW}$ and $R_{\max}^{\text{U2S}} = 50\text{ Mbps}$ unless specified otherwise. For the computing parameters, we set $\alpha = 100\text{ CPU cycles/bit}$, and $\beta = 50\text{ CPU cycles/bit}$. Unless specified otherwise, the maximal CPU frequency of the MEC server is set as $F_{\max} = 5\text{ GHz}$.

For control parameters, unless specified otherwise, the state matrices \mathbf{A}_k are assumed to be 50×50 diagonal matrices with diagonal elements randomly selected in $[-10, 10]$. The control

$$\text{s.t. } \sum_{k=1}^K p_k \leq P_{\max}, \quad (35b)$$

$$\sum_{k=1}^K f_k \leq F_{\max}, \quad (35c)$$

$$\sum_{k=1}^K R_k \leq R_{\max}^{\text{U2S}} \quad (35d)$$

$$\bar{T}_k^{\text{comp},*}(f_k, R_k|f_k^{(i-1)}, R_k^{(i-1)}) + T_k^{\text{commu}} \leq T_k, \quad k = 1, 2, \dots, K, \quad (35e)$$

$$BR_k^{\text{U2G}}(p_k) \geq \frac{\bar{e}_k(l_k)}{T_k^{\text{commu}}}, \quad k = 1, 2, \dots, K, \quad (35f)$$

where i denotes the iteration index, and $f_k^{(i-1)}$ and $R_k^{(i-1)}$ denote the solutions in the $(i-1)$ -th iteration. As $\bar{T}_k^{\text{comp},*}(f_k, R_k|f_{k0}, R_{k0})$ is a convex function, it can be proven that problem (35) is a convex optimization problem, which can be solved efficiently with convex optimization toolboxes [43].

By solving the optimization problem in (35) iteratively, we propose **Algorithm 1** to solve (24). The convergence of this

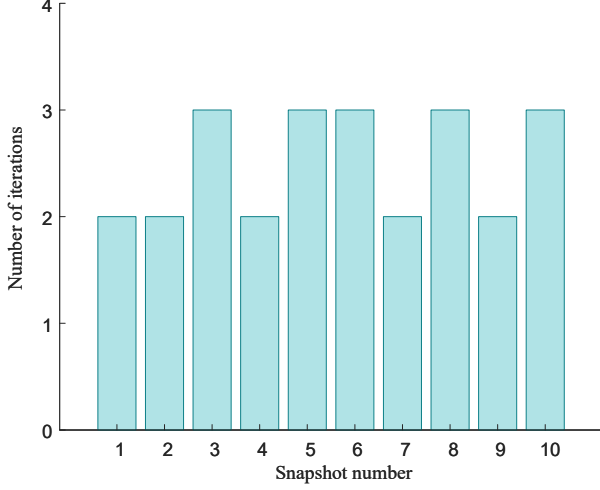


Fig. 3. Convergence performance of the proposed scheme.

system noise and sensing noise are assumed to be independent Gaussian random variables with zero means and covariance matrices $\Sigma_k^V = \sigma_{V,k}^2 \times \mathbf{I}_n$ and $\Sigma_k^W = \sigma_{W,k}^2 \times \mathbf{I}_n$, where $n = 50$, $\sigma_{V,k}^2 = \sigma_V^2 = 0.01$ and $\sigma_{W,k}^2 = \sigma_W^2 = 0.001$ unless otherwise specified. The time duration of each control cycle is set as 70 ms. The observation matrices are set as identity matrices, and the LQR weight matrices are $\mathbf{Q}_k = \mathbf{I}_n, \mathbf{R}_k = \mathbf{0}$.

All the simulations are implemented in MATLAB R2021b, and the convex optimization problem is solved with the `fmincon` function of the Optimization Toolbox. The convergence tolerance threshold is set to be $\epsilon = 5e - 5$.

In order to evaluate the performance of the proposed algorithm, we compare it with the following benchmarks through simulation.

- Closed-loop-oriented power allocation: allocating the EIH transmit power to robots, aiming to minimize the sum LQR cost as in [7], where the computing capability and the satellite-backhaul rate are allocated equally to the loops.
- Communication-oriented scheme: allocating the computing capability of MEC server, aiming to minimize the sum computation time [47], where the satellite-backhaul rate is allocated equally to the loops, then allocating the transmit power of the EIH to robots to maximize the downlink data throughput.

Fig. 3 verifies the convergence performance of the proposed algorithm. Ten snapshots with different robot locations are evaluated, where the transmit power constraint is set as $P_{\max} = 10$ dBW. This figure shows that our proposed algorithm can converge within three iterations, confirming its efficiency in practical applications.

In Fig. 4, we compare the LQR cost achieved by the above three schemes with different transmit power constraints. From this figure, it is seen that the communication-oriented scheme achieves the worst closed-loop performance. Particularly, the system with the communication-oriented scheme will be un-

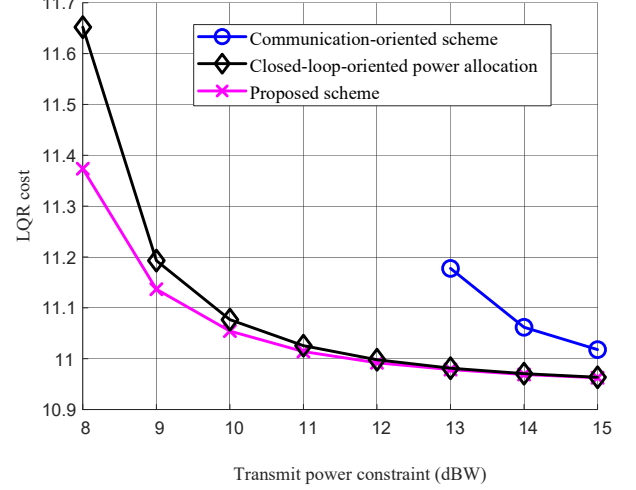


Fig. 4. The LQR cost achieved with different transmit power constraints.

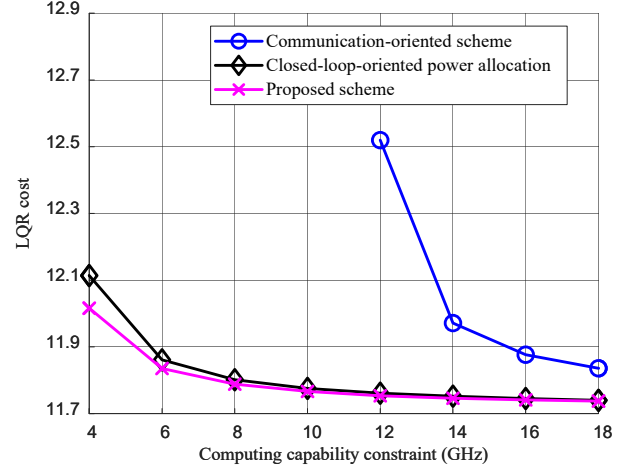


Fig. 5. The LQR cost achieved with different computing capability constraints.

stable when the transmit power constraint is below 12 dBW, leading to an infinite LQR cost. The proposed scheme achieves the lowest LQR cost. In addition, it is shown that the LQR cost is decreasing with respect to the transmit power constraint, which indicates that improving the communication capability is beneficial for the overall closed-loop performance. However, when the transmit power is sufficiently large, the LQR cost becomes saturated, and its decreasing rate slows down.

In Figs. 5 and 6, we show the LQR cost with different computing capability constraints F_{\max} and satellite-backhaul rate constraints R_{\max} , respectively. We can see that the proposed scheme outperforms the other two schemes under all conditions. Similar to Fig. 4, it is shown that the LQR cost is decreasing with respect to the F_{\max} and R_{\max} , indicating that increasing the computing capability can improve the closed-loop control performance of SC^3 loops.

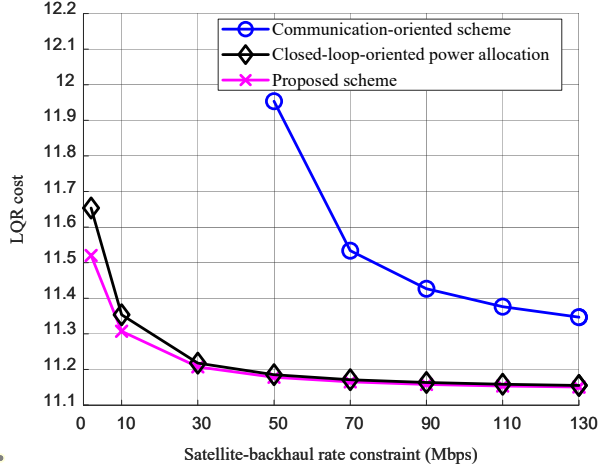


Fig. 6. The LQR cost achieved with different satellite-backhaul rate constraints.

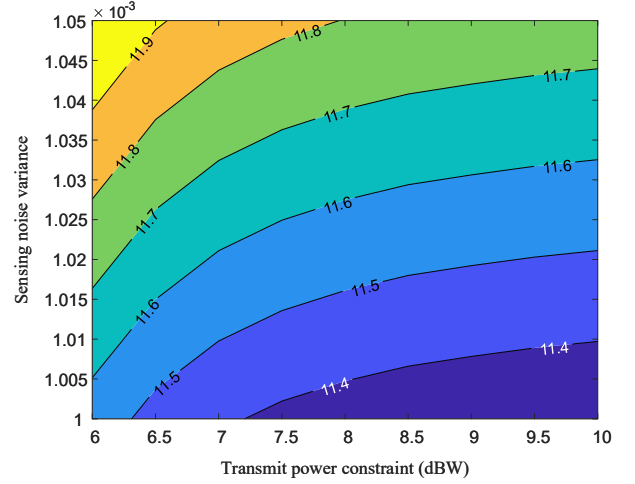


Fig. 8. LQR cost achieved with different transmit power constraints and sensing noise variance.

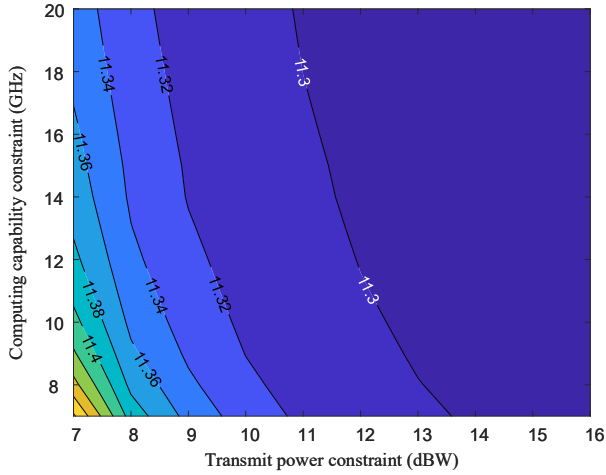


Fig. 7. LQR cost achieved with different transmit power and computing capability constraints.

Fig. 7 shows how the LQR cost is influenced by the transmit power and computing capability on the EIH with the proposed scheme. It is shown that the LQR cost decreases with both the transmit power and computing capability constraints. However, the contours become sparse as the transmit power constraint or computing capability constraint increases, indicating diminishing marginal returns with respect to transmit power and computing capability. In addition, it can be seen that even for the computing capability with a high value, the LQR cost is still restricted by a lower bound that is determined by the maximum power. The reason is that the transmission time T_k^{commu} cannot increase infinitely with the increased computing capability, leading to an upper bound of the transmitted information entropy. The finite information entropy determines the bound of LQR cost l_k , as shown in the constraint (18g).

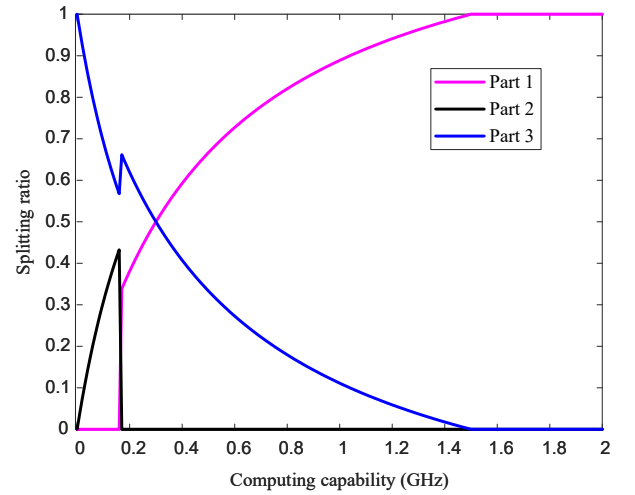


Fig. 9. Optimal splitting ratio of the different parts of sensor data with different computing capabilities.

To show the joint influence of the sensing and communication capability on the closed-loop performance, we show the contours of the sum LQR cost with respect to the transmit power constraint P_{\max} and the sensing noise variance σ_V^2 in Fig. 8. It is shown that the increase of the sensor noise variance will cause the degradation of the control performance, leading to a higher LQR cost. This degradation can be compensated partially by enhancing the communication capability, i.e., increasing P_{\max} . However, even if the transmit power constraint becomes high enough, the LQR cost will still be bounded by the lower bound $l_{\min,k}$, which will also be increased by the sensing part. This result shows that only enhancing the communication capability on the EIH can not fully compensate for the poor sensing ability in the SC^3 loop.

Fig. 9 shows the optimal data splitting vector of the different

parts of sensor data in \mathbf{SC}^3 loop k with different computing capabilities f_k based on **Proposition 1**, where $R_k = 50$ Mbps and $\rho = 0.25$. It can be seen that when the local computing is low, most sensor data will be transmitted to the cloud center for processing (Part 3), and the local computing capability will be fully used on pre-processing the sensor data (Part 2). As the computing capability increases, the sensor data will be either processed locally on the MEC server (Part 1) or on the cloud center (Part 3). Finally, when the local computing capability on the EIH is large enough, all the sensor data will be processed locally, and we have $D_{k,1} = D_k$, and $D_{k,2} = D_{k,3} = 0$.

V. CONCLUSION

In this paper, we investigated an EIH-empowered satellite-UAV network, to serve multiple robots for their control tasks. The UAV-mounted EIH is integrated with sensing, computing, and communication modules. It is capable of directing the behaviors of robots, via synergistic \mathbf{SC}^3 closed-loop orchestration. In order to explore the potential of closed-loop optimization, we have formulated a sum LQR cost minimization problem that jointly optimized the splitting of sensor data, the computing capability, the satellite-backhaul rate, and the transmit power from EIH to robots. An iterative algorithm was proposed to solve this non-convex optimization problem. Simulation results have demonstrated the superiority of the proposed algorithm. Moreover, we have shown the joint influences of the sensing, communication, and computing capability on the sum LQR cost, to uncover a more systematic understanding of closed-loop controls.

APPENDIX A

PROOF OF PROPOSITION 1

First, if $f_k \geq \frac{\alpha D_k}{4\tau}$, all the sensor data should be processed locally on the MCE server of the EIH, and the overall computation time is $T_k^{\text{comp}} = T_{k,1}^{\text{comp}} = \frac{\alpha D_k}{f_k} < 4\tau$. Otherwise, if some sensor data are transmitted to the cloud center through satellite, i.e., $D_{k,2} > 0$ or $D_{k,3} > 0$, the computation time will be larger than the sum propagation delay 4τ , as shown in (5) and (6).

Next, we consider the case of $f_k < \frac{\alpha D_k}{4\tau}$. Based on (2), (5) and (6), we can see that the latency is non-increasing with respect to the $f_{k,1}$, $f_{k,2}$, $R_{k,1}$ and $R_{k,2}$. Therefore, the equality of (20c) and (20d) must hold to minimize the overall computing time, i.e.,

$$f_{k,1} + f_{k,2} = f_k, \quad (36)$$

$$R_{k,2} + R_{k,3} = R_k. \quad (37)$$

Therefore, we have six equations in total, as shown in (1), (21), (22), (36), and (37). Based on these equations, next, we will remove the other variables and express the objective function of (20) as a function of $f_{k,2}$.

From (36), (37) and (22), we have $f_{k,1} = f_k - f_{k,2}$, $R_{k,2} = \frac{\rho}{\beta} f_{k,2}$ and $R_{k,3} = R_k - \frac{\rho}{\beta} f_{k,2}$. Substituting these variables into (20b) and (??), we can get the relation between T_k^{comp} and $f_{k,2}$, formulated as

$$T_k^{\text{comp}} = \frac{\alpha\beta D_k - 4\beta\tau f_k + 4\beta\tau f_{k,2}}{(\alpha - \alpha\rho - \beta)f_{k,2} + \beta f_k + \alpha\beta R_k} + 4\tau. \quad (38)$$

From (38), we see that T_k^{comp} is a fractional linear function of $f_{k,2}$. Therefore, T_k^{comp} is monotonous with respect to $f_{k,2}$. It can be shown that T_k^{comp} is increasing with respect to $f_{k,2}$ if $4\beta\tau R_k - (\alpha - \alpha\rho - \beta)D_k + 4(1 - \rho)\tau f_k \geq 0$, and T_k^{comp} is decreasing otherwise.

Based on the above analysis, if $4\beta\tau R_k - (\alpha - \alpha\rho - \beta)D_k + 4(1 - \rho)\tau f_k \geq 0$, then $f_{k,2}$ should be as small as possible in order to minimize T_k^{comp} . Therefore, we have $f_{k,2} = 0$ in such case. Substituting $f_{k,2} = 0$ into (38), we have

$$T_k^{\text{comp}} = \frac{\alpha D_k - 4\tau f_k}{f_k + \alpha R_k} + 4\tau. \quad (39)$$

On the other hand, if $4\beta\tau R_k - (\alpha - \alpha\rho - \beta)D_k + 4(1 - \rho)\tau f_k \leq 0$, then $f_{k,2}$ should be as large as possible. There are two constraints for $f_{k,2}$, i.e., $f_{k,2} \leq f_k$ and $R_{k,2} = \frac{\rho}{\beta} f_{k,2} \leq R_k$, which indicates that $f_{k,2} = \min\left\{f_k, \frac{\beta R_k}{\rho}\right\}$. Therefore, when $f_k \leq \frac{\beta R_k}{\rho}$, we have $f_{k,2} = f_k$, and

$$T_k^{\text{comp}} = \frac{\beta D_k}{\beta R_k + (1 - \rho)f_k} + 4\tau. \quad (40)$$

On the other hand, if $f_k \geq \frac{\beta R_k}{\rho}$, then $f_{k,2} = \frac{\beta R_k}{\rho}$, $R_{k,2} = R_k$, and

$$T_k^{\text{comp}} = \frac{\rho\alpha D_k - 4\rho\tau f_k + 4\beta R_k\tau}{\rho f_k + (m - \beta)R_k} + 4\tau. \quad (41)$$

Based on the above analysis, the validity of **Proposition 1** has been demonstrated.

APPENDIX B

PROOF OF LEMMA 2

According to [43, Page 89], a function is convex if and only if its epigraph is a convex set, where the epigraph of $f(x, y)$ is defined as $\text{epi}f = \{(x, y, z) | (x, y) \in \text{dom}f, f(x, y) \leq z\}$.

In order to show the convexity of $f(x, y)$, we will show that its epigraph \mathcal{A} is a convex set, which can be formulated as

$$\mathcal{A} = \left\{ (x, y, z) \mid \frac{1}{y} \log \left(1 + \frac{1}{x - a} \right) \leq z, x > a, y > 0 \right\}, \quad (42)$$

We can transform \mathcal{A} to an equivalent form as

$$\mathcal{A} = \left\{ (x, y, z) \mid \frac{1}{\exp(yz) - 1} + a \leq x, y > 0, z > 0 \right\}. \quad (43)$$

From (43), it can be seen that \mathcal{A} can be regarded as the epigraph of a new function $g(y, z) = \frac{1}{\exp(yz) - 1} + a$ with the domain $y > 0, z > 0$.

Next, we show that $g(y, z)$ is convex by checking its Hessian matrix, which is calculated as

$$\nabla^2 g(y, z) = \begin{bmatrix} \frac{z^2 e^{yz} (e^{yz} + 1)}{(e^{yz} - 1)^3} & \frac{e^{yz} (yz - e^{yz} + yz e^{yz} + 1)}{(e^{yz} - 1)^3} \\ \frac{e^{yz} (yz - e^{yz} + yz e^{yz} + 1)}{(e^{yz} - 1)^3} & \frac{y^2 e^{yz} (e^{yz} + 1)}{(e^{yz} - 1)^3} \end{bmatrix}. \quad (44)$$

The determinant of $\nabla^2 g(y, z)$ can be calculated as

$$|\nabla^2 g(y, z)| = \frac{e^{2yz} (2yz e^{yz} - e^{yz} + 2yz + 1)}{(e^{yz} - 1)^5}. \quad (45)$$

It can be shown that $2yz e^{yz} - e^{yz} + 2yz + 1 > 0$ when $y > 0, z > 0$ by checking the derivative. Therefore, we have $|\nabla^2 g(y, z)| > 0$. As $\frac{\partial^2 g}{\partial y^2} > 0$ and $\frac{\partial^2 g}{\partial z^2} > 0$, we can obtain that $\nabla^2 g(y, z)$ is positive definite with $y > 0$ and $z > 0$, which shows the convexity of g . From the above analysis, we have \mathcal{A} is a convex set, indicating that $f(x, y)$ is a convex function.

APPENDIX C PROOF OF LEMMA 4

We first prove the convexity of $\bar{T}_k^{\text{comp},*}(f_k, R_k | f_{k0}, R_{k0})$. As all of $T_k^1(f_k, R_k)$, $\bar{T}_k^2(f_k, R_k | f_{k0}, R_{k0})$, $\bar{T}_k^3(f_k, R_k | f_{k0}, R_{k0})$ and $T_k^4(f_k, R_k)$ are reciprocal functions of the linear combination of f_K and R_k , they are all convex functions. As the point-wise maximum function of two convex functions is still convex function [43], we can establish the convexity of $\bar{T}_k^{\text{comp},*}(f_k, R_k | f_{k0}, R_{k0})$.

Next, we prove the correctness of inequality (34) by comparing the values of $T_k^i(f_k, R_k)$ for $i \in [1, 2, 3, 4]$. The differences of the four functions can be formulated as

$$\begin{aligned} & T_k^1(f_k, R_k) - T_k^2(f_k, R_k) \\ &= \frac{(\rho f_k - \beta R_k) [4(1-\rho)\tau f_k - (\alpha - \alpha\rho - \beta)D_k + 4\beta\tau R_k]}{[\beta R_k + (1-\rho)f_k][\rho f_k + (\alpha - \beta)R_k]}, \end{aligned} \quad (46)$$

$$\begin{aligned} & T_k^1(f_k, R_k) - T_k^3(f_k, R_k) \\ &= \frac{f_k [4(1-\rho)\tau f_k - (\alpha - \alpha\rho - \beta)D_k + 4\beta\tau R_k]}{[\beta R_k + (1-\rho)f_k](f_k + \alpha R_k)}, \end{aligned} \quad (47)$$

$$\begin{aligned} & T_k^2(f_k, R_k) - T_k^3(f_k, R_k) \\ &= \frac{\alpha R_k [4(1-\rho)\tau f_k - (\alpha - \alpha\rho - \beta)D_k + 4\beta\tau R_k]}{(f_k + \alpha R_k)[\rho f_k + (\alpha - \beta)R_k]}, \end{aligned} \quad (48)$$

$$\begin{aligned} & T_k^3(f_k, R_k) - T_k^4(f_k, R_k) \\ &= \frac{\alpha R_k (4f_k\tau - \alpha D_k)}{f_k(f_k + \alpha R_k)}. \end{aligned} \quad (49)$$

Based on the above results, we can establish the relationship among the four functions when (f_k, R_k) falls in different areas, that is

$$T_k^4(f_k, R_k) > T_k^3(f_k, R_k) > T_k^1(f_k, R_k), \quad (f_k, R_k) \in \mathcal{S}_1 \quad (50a)$$

$$T_k^4(f_k, R_k) > T_k^3(f_k, R_k) \geq T_k^2(f_k, R_k), \quad (f_k, R_k) \in \mathcal{S}_2 \quad (50b)$$

$$T_k^1(f_k, R_k) \geq T_k^2(f_k, R_k) \geq T_k^3(f_k, R_k), \quad (f_k, R_k) \in \mathcal{S}_3 \quad (50c)$$

$$T_k^4(f_k, R_k) \geq T_k^3(f_k, R_k), \quad (f_k, R_k) \in \mathcal{S}_3 \quad (50d)$$

$$T_k^2(f_k, R_k) \geq T_k^3(f_k, R_k) > T_k^4(f_k, R_k), \quad (f_k, R_k) \in \mathcal{S}_4 \quad (50e)$$

With the inequalities in (50), it can be proven that, for any $f_k \geq 0, R_k \geq 0$, the following inequalities hold

$$T_k^{\text{comp},*}(f_k, R_k) \leq \max\{T_k^1(f_k, R_k), T_k^2(f_k, R_k)\}, \quad (51a)$$

$$T_k^{\text{comp},*}(f_k, R_k) \leq T_k^3(f_k, R_k), \quad (51b)$$

$$T_k^{\text{comp},*}(f_k, R_k) \leq T_k^4(f_k, R_k). \quad (51c)$$

Therefore, if $(f_{k0}, R_{k0}) \in \mathcal{S}_1 \cup \mathcal{S}_2$, we have

$$\bar{T}_k^{\text{comp},*}(f_k, R_k | f_{k0}, R_{k0}) \quad (52a)$$

$$= \max\{T_k^1(f_k, R_k), \bar{T}_k^2(f_k, R_k | f_{k0}, R_{k0})\} \quad (52b)$$

$$\geq \max\{T_k^1(f_k, R_k), T_k^2(f_k, R_k)\} \quad (52c)$$

$$\geq T_k^{\text{comp},*}, \quad (52d)$$

where (52b) is based on the definition of $\bar{T}_k^{\text{comp},*}$ in (29), (52c) follows from (27) and (28), and (52d) follows from (51a)

If $(f_{k0}, R_{k0}) \in \mathcal{S}_3$ or $(f_{k0}, R_{k0}) \in \mathcal{S}_4$, it can be proven that $\bar{T}_k^{\text{comp},*}(f_k, R_k | f_{k0}, R_{k0}) \geq T_k^{\text{comp},*}(f_k, R_k)$ following a similar procedure as (52), which demonstrates the correctness of (34)

Finally, we show the equality condition of (34), i.e.,

$$\bar{T}_k^{\text{comp},*}(f_{k0}, R_{k0} | f_{k0}, R_{k0}) = T_k^{\text{comp},*}(f_{k0}, R_{k0}). \quad (53)$$

If $(f_k, R_k) \in \mathcal{S}_1$, we have

$$\bar{T}_k^{\text{comp},*}(f_{k0}, R_{k0} | f_{k0}, R_{k0}) \quad (54a)$$

$$= \max\{T_k^1(f_{k0}, R_{k0}), \bar{T}_k^2(f_{k0}, R_{k0} | f_{k0}, R_{k0})\} \quad (54b)$$

$$= \max\{T_k^1(f_{k0}, R_{k0}), T_k^2(f_{k0}, R_{k0})\} \quad (54c)$$

$$= T_k^1(f_{k0}, R_{k0}) \quad (54d)$$

$$= T_k^{\text{comp},*}(f_{k0}, R_{k0}), \quad (54e)$$

where (54d) follows from (46). If (f_k, R_k) falls into other areas, the equality can be proven in a similar way, which completes the proof.

APPENDIX D PROOF OF PROPOSITION 2

Denoting the optimal solution to problem (35) in the i -th iteration as $(\mathbf{p}^i, \mathbf{f}^i, \mathbf{R}^i, \mathbf{l}^i, \mathbf{T}^{\text{commu},i})$, we have

$$T_k^{\text{comp},*}(f_k^i, R_k^i) + T_k^{\text{commu}} \quad (55a)$$

$$\leq \bar{T}_k^{\text{comp},*}(f_k^i, R_k^i | f_k^{(i-1)}, R_k^{(i-1)}) + T_k^{\text{commu}} \quad (55b)$$

$$\leq T_k, \quad (55c)$$

holds for $k = 1, 2, \dots, K$, where (55a) follows from (34), and (55b) follows from (35e). Therefore, any optimal solution to (35) will also satisfy all the constraints in (24), i.e., (24b)-(24f), indicating that it is also a feasible solution to (24).

Next, we show the convergence of **Algorithm 1**. We have

$$\bar{T}_k^{\text{comp},*}(f_k^{(i-1)}, R_k^{(i-1)} | f_k^{(i-1)}, R_k^{(i-1)}) + T_k^{\text{commu}} \quad (56a)$$

$$= T_k^{\text{comp},*}(f_k^{(i-1)}, R_k^{(i-1)}) + T_k^{\text{commu}} \quad (56b)$$

$$\leq \bar{T}_k^{\text{comp},*}(f_k^{(i-1)}, R_k^{(i-1)} | f_k^{(i-2)}, R_k^{(i-2)}) + T_k^{\text{commu}} \quad (56c)$$

$$\leq T_k, \quad (56d)$$

where (56c) follows from (34), and (56d) holds because \mathbf{f}^{i-1} and \mathbf{R}^{i-1} are the optimal solution to (35) in the $(i-1)$ -th iteration and should satisfy the constraint (35e). Therefore, it is shown that $(\mathbf{p}^{(i-1)}, \mathbf{f}^{(i-1)}, \mathbf{R}^{(i-1)}, \mathbf{l}^{(i-1)}, \mathbf{T}^{\text{commu},(i-1)})$ is also feasible to the optimization problem (35) in the i -th iteration, indicating that $L^{(i-1)}$ is also an achievable objective function value in the i -th iteration. As $(\mathbf{p}^i, \mathbf{f}^i, \mathbf{R}^i, \mathbf{l}^i, \mathbf{T}^{\text{commu},i})$ minimizes (35) in the i -th iteration, we have $L^i \leq L^{(i-1)}$ holds for any $i \geq 1$, which completes the proof.

REFERENCES

- [1] R. Ventura and P. U. Lima, "Search and rescue robots: The civil protection teams of the future," in *Proc. 3rd Int. Conf. IEEE Emerg. Secur. Technol.*, Lisbon, Portugal, 2012, pp. 12-19.
- [2] T. Klamt *et al.*, "Flexible disaster response of tomorrow: Final presentation and evaluation of the CENTAURO system," *IEEE Robot. Automat. Mag.*, vol. 26, no. 4, pp. 59-72, Dec. 2019.
- [3] Q. Huang and J. Jiang, "A radiation-tolerant wireless communication system for severe accident monitoring without relying on rad-hardened electronic components," *Nuclear Technology* vol. 207, no. 5, pp. 711-725, May 2021.
- [4] H. Li and A. V. Savkin, "Wireless sensor network based navigation of micro flying robots in the industrial internet of things," *IEEE Trans. Ind. Informat.*, vol. 14, no. 8, pp. 3524-3533, Aug. 2018.
- [5] V. K. Sarker, J. Peña Queralta, T. N. Gia, H. Tenhunen and T. Westerlund, "Offloading SLAM for indoor mobile robots with edge-fog-cloud computing," in *Proc. 1st Int. Conf. Adv. Sci., Eng. Robot. Technol. (ICASERT)*, Dhaka, Bangladesh, 2019, pp. 1-6.
- [6] Y. Kantaros and M. M. Zavlanos, "Global planning for multi-robot communication networks in complex environments," *IEEE Trans. Robot.*, vol. 32, no. 5, pp. 1045-1061, Oct. 2016.
- [7] C. Lei *et al.*, "Control-oriented power allocation for integrated satellite-UAV networks," *IEEE Wireless Commun. Lett.*, vol. 12, no. 5, pp. 883-887, May 2023.
- [8] F. Zhou, Y. Wu, R. Q. Hu and Y. Qian, "Computation rate maximization in UAV-enabled wireless-powered mobile-edge computing systems," *IEEE J. Sel. Areas Commun.*, vol. 36, no. 9, pp. 1927-1941, Sep. 2018.
- [9] P. McEnroe, S. Wang and M. Liyanage, "A survey on the convergence of edge computing and AI for UAVs: Opportunities and challenges," *IEEE Internet Things J.*, vol. 9, no. 17, pp. 15435-15459, 1 Sep. 2022.
- [10] M. M. Azari *et al.*, "Evolution of non-terrestrial networks from 5G to 6G: A Survey," *IEEE Commun. Surv. Tutor.*, vol. 24, no. 4, pp. 2633-2672, 4th Quart. 2022.
- [11] J. Van de Vegte, *Feedback Control Systems*. 3rd ed. Englewood Cliffs, NJ, USA: Prentice-Hall, 1994.
- [12] G. F. Franklin, J. D. Powell, and A. Emami-Naeini, *Feedback Control of Dynamic Systems*. 6th ed. Englewood Cliffs, NJ: Prentice-Hall, 2009.
- [13] G. A. Leonov, D. V. Ponomarenko, and V. B. Smirnova, *Frequency-Domain Methods for Nonlinear Analysis: Theory and Applications*. Singapore: World Scientific, 1996.
- [14] L. Chua and C. Ng, "Frequency domain analysis of nonlinear systems: General theory," *IEEE J. Electron. Circuits Syst.* vol. 3, no. 4, pp. 165-185, Jul., 1979.
- [15] Z. Bubnicki, *Modern Control Theory*. Berlin, Germany: Springer, 2005.
- [16] M. Gopal, *Modern Control System Theory*. New York, NY, USA: New Age Int., 1993.
- [17] E. B. Lee and L. Markus, *Foundations of Optimal Control Theory*. North Chelmsford, MA, USA: Courier Corporation, 2012.
- [18] D. E. Kirk, *Optimal Control Theory: An Introduction*. New York: Wiley, 1967.
- [19] M. Athans, "The role and use of the stochastic linear-quadratic-Gaussian problem in control system design," *IEEE Trans. Auto. Control*, vol. 16, no. 6, pp. 529-552, Dec. 1971.
- [20] R. E. Kalman "Contributions to the theory of optimal control," *Bol. Soc. Mat. Mexicana*, vol. 5, no. 1, pp. 102-119, 1960.
- [21] G. N. Nair, F. Fagnani, S. Zampieri, and R. J. Evans, "Feedback control under data rate constraints: An overview," *Proc. IEEE*, vol. 95, no. 1, pp. 108-137, Jan. 2007.
- [22] J. P. Hespanha, P. Naghshtabrizi and Y. Xu, "A survey of recent results in networked control systems," *Proc. IEEE*, vol. 95, no. 1, pp. 138-162, Jan. 2007.
- [23] M. S. Mahmoud and M. M. Hamdan, "Fundamental issues in networked control systems," *IEEE/CAA J. Automatica Sinica*, vol. 5, no. 5, pp. 902-922, Sep. 2018.
- [24] M. S. Branicky, S. M. Phillips, and W. Zhang, "Stability of networked control systems: Explicit analysis of delay" in *Proc. Amer. Contr. Conf.*, Chicago, USA, Jun. 2000, vol. 4, pp. 2352-2357.
- [25] Y. Feng, X. Chen and G. Gu, "Output feedback stabilization for discrete-time systems under limited communication," *IEEE Trans. Auto. Control*, vol. 62, no. 4, pp. 1927-1932, Apr. 2017.
- [26] C. Tan, H. Sui, Y. Li, Z. Zhang and W. S. Wong, "Integrated stabilizing control for sampled-data NCSs with intermittent observation and multiple random transmission delays," *IEEE Trans. Control Netw. Syst.*, vol. 10, no. 4, pp. 2035-2047, Dec. 2023.
- [27] D. E. Quevedo, E. I. Silva and G. C. Goodwin, "Control over unreliable networks affected by packet erasures and variable transmission delays," *IEEE J. Sel. Areas Commun.*, vol. 26, no. 4, pp. 672-685, May 2008.
- [28] D. Yue, E. Tian and Q. -L. Han, "A delay system method for designing event-triggered controllers of networked control systems," *IEEE Trans. Auto. Control*, vol. 58, no. 2, pp. 475-481, Feb. 2013.
- [29] K. Gatsis, A. Ribeiro and G. J. Pappas, "Optimal power management in wireless control systems," *IEEE Trans. Auto. Control*, vol. 59, no. 6, pp. 1495-1510, Jun. 2014.
- [30] T. Soleymani, J. S. Baras, S. Hirche, and K. H. Johansson, "Value of information in feedback control: Global optimality," *IEEE Trans. Auto. Control*, vol. 68, no. 6, pp. 3641-3647, Jun. 2023.
- [31] Y. Qiao, Y. Fu and M. Yuan, "Communication-control co-design in wireless networks: A cloud control AGV example," *IEEE Internet Things J.*, vol. 10, no. 3, pp. 2346-2359, Feb. 2023.
- [32] V. Kostina and B. Hassibi, "Rate-cost tradeoffs in control," *IEEE Trans. Auto. Control*, vol. 64, no. 11, pp. 4525-4540, Nov. 2019.
- [33] T. Nguyen, L. Y. Wang, G. Yin, H. Zhang, S. E. Li and K. Li, "Impact of communication erasure channels on control performance of connected and automated vehicles," *IEEE Trans. Veh. Technol.*, vol. 67, no. 1, pp. 29-43, Jan. 2018.
- [34] M. Barforooshan, M. S. Derpich, P. A. Stavrou and J. Østergaard, "The effect of time delay on the average data rate and performance in networked control systems," *IEEE Trans. Auto. Control*, vol. 67, no. 1, pp. 16-31, Jan. 2022.
- [35] B. Chang, L. Zhang, L. Li, G. Zhao and Z. Chen, "Optimizing resource allocation in URLLC for real-time wireless control systems," *IEEE Trans. Veh. Technol.*, vol. 68, no. 9, pp. 8916-8927, Sep. 2019.
- [36] P. M. de Sant Ana, N. Marchenko, P. Popovski and B. Soret, "Control-aware scheduling optimization of industrial IoT," in *Proc. IEEE 95th Veh. Technol. Conf. (VTC-Spring)*, Helsinki, Finland, 2022, pp. 1-6.
- [37] Q. Hu, Y. Cai, G. Yu, Z. Qin, M. Zhao and G. Y. Li, "Joint offloading and trajectory design for UAV-enabled mobile edge computing systems" *IEEE Internet Things J.*, vol. 6, no. 2, pp. 1879-1892, Apr. 2019.
- [38] H. Peng and X. Shen, "Multi-agent reinforcement learning based resource management in MEC- and UAV-assisted vehicular networks," *IEEE J. Sel. Areas Commun.*, vol. 39, no. 1, pp. 131-141, Jan. 2021.
- [39] Y. Ding *et al.*, "Online edge learning offloading and resource management for UAV-assisted MEC secure communications," *IEEE J. Sel. Topics in Signal Process.*, vol. 17, no. 1, pp. 54-65, Jan. 2023.
- [40] X. Dai, Z. Xiao, H. Jiang and J. C. S. Lui, "UAV-assisted task offloading in vehicular edge computing networks," *IEEE Trans. Mobile Comput.* early access, 2023.
- [41] Y. Zeng, R. Zhang, and T. J. Lim, "Throughput maximization for UAV-enabled mobile relaying systems," *IEEE Trans. Commun.*, vol. 64, no. 12, pp. 4983-4996, Dec. 2016.
- [42] E. D. Sontag, *Mathematical Control Theory: Deterministic Finite Dimensional Systems*. New York, NY, USA: Springer Science & Business Media, 2013.
- [43] S. Boyd and L. Vandenberghe, *Convex Optimization*. Cambridge, U.K.: Cambridge Univ. Press, 2004.
- [44] Y. Sun, P. Babu and D. P. Palomar, "Majorization-minimization algorithms in signal processing, communications, and machine learning," *IEEE Trans. Signal Process.*, vol. 65, no. 3, pp. 794-816, Feb. 2017.
- [45] Y. Du, K. Yang, K. Wang, G. Zhang, Y. Zhao and D. Chen, "Joint resources and workflow scheduling in UAV-enabled wirelessly-powered MEC for IoT systems," *IEEE Trans. Veh. Technol.*, vol. 68, no. 10, pp. 10187-10200, Oct. 2019.
- [46] M. Hua, Y. Wang, Z. Zhang, C. Li, Y. Huang, and L. Yang, "Power-efficient communication in UAV-aided wireless sensor networks," *IEEE Commun. Lett.*, vol. 22, no. 6, pp. 1264-1267, Jun. 2018.
- [47] J. Ren, G. Yu, Y. He and G. Y. Li, "Collaborative cloud and edge computing for latency minimization," *IEEE Trans. Veh. Technol.*, vol. 68, no. 5, pp. 5031-5044, May 2019.